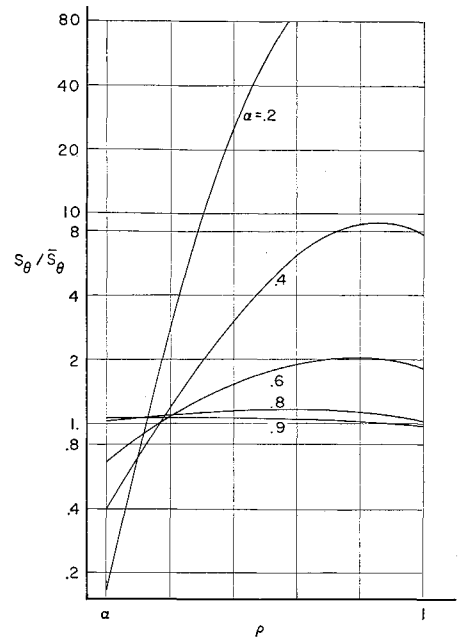

Fig. 3 Tangential stress comparison.

$$\rho^\gamma \frac{d}{d\rho}\left[\rho^{1-2\gamma}\frac{d}{d\rho}(\rho^{1+\gamma}S_r)\right] = \nu_{\theta r}(\lambda-\mu)P + (2+\nu_{\theta r})\mu\rho\frac{dP}{d\rho} + \mu\rho^2\frac{d^2P}{d\rho^2} \quad (7)$$

Equation (7) yields, after two integrations

$$S_r = C_1/\rho^{1-\gamma} + C_2/\rho^{1+\gamma} + \mu P - \mu(1-\nu_{\theta r})/\rho^{1+\gamma} \times \int \rho v^\gamma P(v)dv + [\nu_{\theta r}(\lambda-\mu)(1-\gamma)(\gamma+\nu_{\theta r})]/\rho^{1+\gamma}\int^\rho v^{2+\gamma}\int^v w^{-\gamma}P(w)dwdv, \quad (8)$$

where C_1 and C_2 are integration constants.

The tangential stress and the radial displacement are then found from the expressions

$$S_\theta = \lambda P + (d/d\rho)\,[\rho(\sigma_r - \mu P)], \quad (9a)$$

$$U = \rho(S_\theta - \nu_{\theta r}S_r)p_0/E_\theta \quad (9b)$$

Numerical Example

Consider a circular disc subjected to a pressure p_0 at its inner radius a, which drops linearly to zero at the outer radius, b. Let $L = b$ and $\alpha = a/b$, and assume $\lambda = \mu = 1$. The pressure is then given by

$$P = (1-\rho)/(1-\alpha) \quad (10)$$

Inserting Eq. (10) into Eqs. (8–9b) yields for the radial and tangential stresses and the radial deformation:

$$S_r = (2+\nu_{\theta r})\rho/[(\gamma^2-4)(1-\alpha)] + C_1/\rho^{1-\gamma} + C_2/\rho^{1+\gamma} \quad (11a)$$

$$S_\theta = (\gamma^2+2\nu_{\theta r})\,\rho/[(\gamma^2-4)(1-\alpha)] + \gamma C_1/\rho^{1-\gamma} - \gamma C_2/\rho^{1-\gamma} \quad (11b)$$

$$U = \{(\gamma^2-\nu_{\theta r}{}^2)\rho^2/[(\gamma^2-4)(1-\alpha)] + (\gamma-\nu_{\theta r})C_1\rho^\gamma - (\gamma+\nu_{\theta r})C_2\rho^{-\gamma}\}p_o/E_\theta, \quad (11c)$$

provided $\gamma \neq 2$. If the disk is assumed to be traction free at its inner and outer radius, C_1 and C_2 will yield

$$C_1 = -(2+\nu_{\epsilon r})(\alpha^{\gamma+2}-1)/[(\gamma^2-4)(1-\alpha)(\alpha^{2\gamma}-1)] \quad (12a)$$

$$C_2 = (2+\nu_{\theta r})(\alpha^{\gamma+2}-\alpha^{2\gamma})/[(\gamma-4)(1-\alpha)\,(\alpha^{2\gamma}-1)] \quad (12b)$$

The tangential stresses are plotted for the case $\gamma^2 = 16$ and $\nu_{\theta r} = 1.8$ in Fig. 2 vs ρ, for various values of α. Those values of γ^2 and $\nu_{\theta r}$ are typical for a PYROCERAM glass ceramic matrix structure. When the disk is subjected to an internal pressure p_o only, the tangential stresses are

$$\bar{S}_\theta = \gamma\alpha^{1+\gamma}(1/\rho^{1+\gamma} + 1/\rho^{1-\gamma})/(1-\alpha^{2\gamma}) \quad (13)$$

In Fig. 3, the ratio $S_\theta/\bar{S}_\theta$ is plotted vs ρ, for various values of α. It is seen that S_θ varies considerably from $\bar{S}_\theta$ except in the neighborhood of $\alpha = 1$. In the latter case S_θ and $\bar{S}_\theta$ may be approximated by:

$$S_\theta = (1+\alpha)/[2(1-\alpha)];\ \bar{S}_\theta = \alpha(1-\alpha)^{-1} \quad (14)$$

These expressions are obtained from equilibrium considerations of the disk element in Fig. 1 when dr is replaced by $b-a$ and for r, the average radius $(b+a)/2$ is used.

Heat Transfer in Separated Laminar Hypersonic Flow

J. W. Hodgson*
The University of Tennessee, Knoxville, Tenn.

Nomenclature

c_p = constant pressure specific heat (assumed constant)
L = reattachment zone length
M_e = local freestream Mach number
n = summing index
r = recovery factor ($Pr^{1/2}$ for laminar flow)
Re_L = U_dL/ν_c
Re_w = U_ew/ν_e
S^* = Denison and Baum[6] parameter
S_b = surface distance from leading stagnation point of body to leading edge of cavity
St_y = local Stanton number, $q/[\rho_c v c_p(T_d - T_w)]$
St_L = Stanton number at $y = L$
T_{aw} = freestream laminar adiabatic wall temperature
T_e = local freestream temperature
T_w = cavity wall temperature
U_e = local freestream velocity
v = local velocity outside boundary layer on cavity wall
γ = ratio of specific heats (c_p/c_v)
ρ_c = density in cavity
ν_c = kinematic viscosity in cavity
ν_e = local freestream kinematic viscosity

THE flow of a fluid over and within a cavity formed in a surface has been the subject of much research.[1–9] From these studies it is clear that the floor of the cavity will, in general, experience a lower convective heat flux than would a smooth surface exposed to the same external flow conditions. Hunt and Howell,[1] pursuing means for the thermal protection of hypersonic vehicles, found that adding an open honeycomb structure to a surface significantly decreased the temperature of that surface in hypersonic flow—provided the cell geometry was such that the cell depth was more than twice the cell width. Because most of the previously reported data were obtained for shallow (width greater than depth) cavities, Wieting[2] measured the heat flux distribution in single deep cavities and found good agreement between his data and Burggraf's[3] theory. There remained a need, however, for a

Received August 19, 1970; revision received September 24, 1970. The work on which this paper is based was performed by the author while serving as a NASA-ASEE Summer Faculty Research Fellow with the Structures Research Division at Langley Research Center, Hampton, Va.

* Associate Professor, Mechanical and Aerospace Engineering Department.

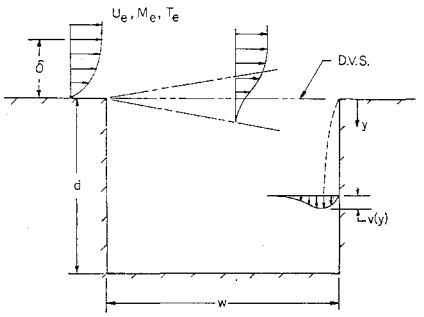

Fig. 1 Flow model.

study that would focus on the reattachment wall and show the influence of the cavity geometry and the oncoming boundary-layer characteristics on the heat-transfer rate in that area. A study by Nestler[4] provided the stimulus for the approach taken in this paper.

The model chosen is shown in Fig. 1 and is similar to that used by Chung and Viegas[5] who neglected the oncoming boundary layer. Although their analysis is for incompressible flow, Burggraf[3] points out that the assumption may be valid because of the low velocities and high temperatures in a cavity exposed to hypersonic flow. The resulting expression for the velocity down the reattachment wall is

$$\frac{v(y)}{U_d} = 1 - 0.189 \exp\left(-5.3\frac{y}{L}\right) - 10.6 \sum_{n=1}^{\infty} \frac{\exp[-y/L(9.87n^2 + 28.1)^{1/2}]}{9.87n^2 + 28.1} \quad (1)$$

The effect of the finite upstream boundary layer is in its influence on the dividing streamline velocity U_d. In this paper, U_d was obtained from the analysis by Denison and Baum[6] who took into account the oncoming boundary layer. A similar analysis that could be used is that by Charwat and Der.[7]

The reattachment wall is thus reduced to the familiar case of heat transfer to a flat plate exposed to an incompressible fluid having a varying freestream velocity. One technique for handling such a flow (Smith and Spalding[10] and summarized by Kays[11]) treats the local flow as an equivalent wedge flow. The resulting expression for the local Stanton number is

$$St_y Re_L^{1/2} = C_1 \left(\frac{v}{U_d}\right)^{C_2} \Big/ \left[\int_0^{y/L} \left(\frac{v}{U_d}\right)^{C_3} d\left(\frac{y}{L}\right)\right]^{1/2} \quad (2)$$

where C_1, C_2, and C_3 depend upon the Prandtl number as shown in Table 1. Since v/U_d is a function of y/L, the right side of Eq. (2) involves only y/L and the Prandtl number.

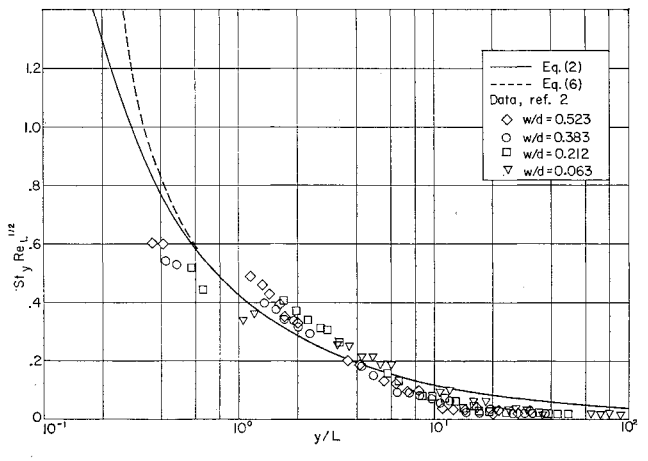

Fig. 2 Heat transfer on the reattachment wall.

Table 1 Constants in Eqs. (2) and (6)

Pr	A	C_1	C_2	C_3
0.7	0.178	0.418	0.435	1.87
0.8	0.180	0.384	0.450	1.90
1.0	0.186	0.332	0.475	1.95

In calculating the fluid properties in the cavity it is assumed that the cavity pressure is essentially the same as the local freestream pressure, and the average cavity temperature $T_c = 0.5(T_d + T_w)$ is also used. The dividing streamline temperature T_d is found using Crocco's relationship modified for Prandtl numbers different from unity[12]

$$T_d = T_w + (U_d/U_e)(T_{aw} - T_w) - (U_d/U_e)^2 r(U_e^2/2c_p) \quad (3)$$

The reattachment zone length L is obtained by correcting the incompressible value L_i defined by[5]

$$L_i = 11.8w/Re_w^{1/2} \quad (4)$$

where w is the width of the cavity. The correction, suggested by Nestler,[4] is obtained from an examination of Chapman's[8] study

$$L = L_i\{1 + [(\gamma - 1)/2]M_e^2[0.447/5.22 + 4.41(T_w/T_e - 1)]\} \quad (5)$$

For values of $y > L$, Eq. (2) can be simplified as in this region $v = U_d$. Under these conditions Eq. (2) becomes

$$St_y Re_L^{1/2} = C_1/(y/L - A)^{1/2} \quad (6)$$

where

$$A = 1 - (C_1^2/St_L^2 Re_L)$$

and is a function of the Prandtl number Pr as shown in Table 1.

Results

A comparison between Eq. (2) for $Pr = 0.8$ and Wieting's[2] data is shown in Fig. 2. The data are for cavities of various width-to-depth ratios, unit freestream Reynolds numbers between 1.4×10^6/ft and 2.3×10^6/ft (4.6×10^6/m and 7.6×10^6/m), nominal freestream Mach numbers of 7, and Prandtl number of 0.75. Also shown is Eq. (6) for $Pr = 0.8$.

Equation (6) can be solved for the local heat-transfer rate q

$$q = \Psi U_d^{1/2} L^{-1/2}(T_d - T_w) \quad (7)$$

where

$$\Psi = (v/U_d)\rho_c c_p \nu_c^{1/2}[C_1/(y/L - A)^{1/2}]$$

For specified fluid properties and y/L location, Ψ is fixed and the influence of the cavity depth d, the cavity width w, and the oncoming boundary-layer thickness δ, can be determined from Eq. (7).

The cavity depth d theoretically has no effect on the heating rate to the downstream wall. As the cavity depth is increased, however, the floor is subjected to lower convective heat loads. If the cavity depth is too shallow, the flow coming off the downstream wall may cause locally high-heating rates on the floor, caused by the stagnation-like conditions formed. This effect was observed by Hahn[9] in experiments involving shallow cavities.

The cavity width w influences U_d (and thus, T_d) and L. For small cavities exposed to thick boundary layers ($S^* < 0.01$), U_d is proportional to $w^{1/3}$ (and thus, $T_d - T_w$ is approximately proportional to $w^{1/3}$) and L is proportional to $w^{1/2}$. The net result is that the heat-transfer rate for a given y/L is proportional to $w^{1/4}$. Since w also affects Ψ (through L) the net result is that increases in w result in increases in

the heat-transfer rate. The effect becomes less noticeable, however, as y increases.

The oncoming boundary-layer thickness δ is expressed indirectly by S^* and its main effect is found in its influence on the dividing streamline velocity U_d. For the case of constant external flow conditions, S^* is proportional to w/S_b. Also under these conditions δ is proportional to $S_b^{1/2}$. Thus, S^* is proportional to δ^{-2} and (if $S^* < 0.01$) U_d and $T_d - T_w$ are both proportional to $\delta^{-2/3}$. The net result is that the local heat-transfer rate is proportional to $\delta^{-4/3}$. That is, increases in the oncoming boundary-layer thickness will decrease the convective heat-transfer rate within the cavity.

References

[1] Hunt, L. R. and Howell, R. R., "Exploratory Study of Open-Face Honeycomb to Reduce Temperature of Hypersonic Aircraft Structure," TN D-5278, 1969, NASA.

[2] Wieting, A. R., "Experimental Investigation of Heat Transfer Distributions in Deep Cavities in Hypersonic Separated Flow," TN D-5908, 1970, NASA.

[3] Burggraf, O. R., "A Model of Steady Separated Flow in Rectangular Cavities at High Reynolds Number," *Proceedings of the 1965 Heat Transfer and Fluid Mechanics Institute*, 1965, Stanford University Press, Stanford, Calif. pp. 190–229.

[4] Nestler, D. E., "Laminar Heat Transfer to Cavities in Hypersonic Low Density Flow," *Proceedings of the Third International Heat Transfer Conference*, American Society of Mechanical Engineers, Vol. II, 1966, pp. 251–261.

[5] Chung, P. M. and Viegas, J. R., "Heat Transfer at the Reattachment Zone of Separated Laminar Boundary Layers," TN D-1072, 1961, NASA.

[6] Denison, M. R. and Baum, E., "Compressible Free Shear Layer with Finite Initial Thickness," *AIAA Journal*, Vol. I, No. 2, Feb. 1963, pp. 342–349.

[7] Charwat, A. F. and Der, J., Jr., "Studies on Laminar and Turbulent Free Shear Layers with a Finite Initial Boundary Layer at Separation," CP 4, 1966, AGARD, pp. 215–240.

[8] Chapman, D. R., "A Theoretical Analysis of Heat Transfer in Regions of Separated Flow," TN 3792, 1956, NACA.

[9] Hahn, M., "Experimental Investigation of Separated Flow Over a Cavity at Hypersonic Speed," AIAA Paper 68-672, Los Angeles, 1968.

[10] Smith, A. G. and Spalding, D. B., "Heat Transfer in a Laminar Boundary Layer with Constant Fluid Properties and Constant Wall Temperature," *Journal of the Royal Aeronautical Society*, Vol. 62, Jan. 1958, pp. 60–64.

[11] Kays, W. M., *Convective Heat and Mass Transfer*, 1st ed., McGraw-Hill, New York, 1966, pp. 223–226.

[12] Schlichting, H., *Boundary-Layer Theory*, 6th ed., McGraw-Hill, New York, 1968, p. 322.

Transient Nonlinear Deflections of a Cantilever Beam of Uniformly Varying Length by Numerical Methods

ARMAND L. DILPARE*

Lundy Electronics & Systems, Inc., Glen Head, N.Y.

Introduction

THE exoatomospheric deployment of a long slender radio antenna from an accelerating space vehicle may be dynamically idealized as a cantilever beam of uniformly varying length in a constant gravity field (Fig. 1). The dynamics problem consists in determining, at any instant of time, the relative position and velocity vectors of every point along the beam, i.e., the instantaneous deflection and velocity distribution curves. Qualitatively, if the beam is fairly stiff, and deployment is slow, then the transient deflection curve will be close to the static deflection curve associated with the unsupported length at that instant. Conversely, if the beam is very flexible and/or deployment is rapid, the deflection of the free end will approach the $\frac{1}{2}gt^2$ value.

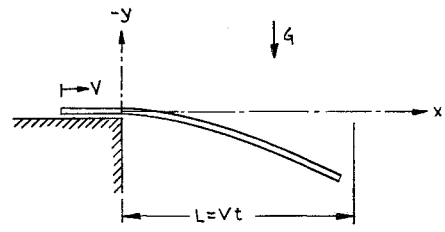

Fig. 1 Antenna deployment geometry.

A numerical method of solution is applied to this problem because deflections and slopes are expected to be large, well into the nonlinear region; and the antenna is nonuniform with a discontinuous distribution of mass and stiffness. The continuous beam structure is replaced with an equivalent lumped-parameter system of elastically coupled rigid bars.[1–4] The accuracy of the approximation improves with an increasing number of bars in the equivalent system. For the present, an equivalent system of six bars has been selected as a compromise between accuracy and computational time.

Equations of Motion for Equivalent System

As shown in Fig. 2, $R_1, R_2, \ldots, R_6$ are the lengths of the beam segments selected so that each segment has uniform properties, i.e., up to five discontinuities may be accommodated. Each segment is replaced with an elastic hinge at its center connecting rigid bars leading to the adjoining segments. The hinge spring constants (K_j) correspond to the rotational deflection of an individual segment under uniform bending moment, i.e.,

$$K_j = E_j I_j / R_j$$

The rigid bars ($S_1, S_2, \ldots, S_6$) have lengths calculated

$$S_1 = \tfrac{1}{2}R_1$$

$$S_j = \tfrac{1}{2}(R_j + R_{j-1}); \quad j > 2$$

and the corresponding masses

$$m_j = \tfrac{1}{2}(\text{mass of } R_j + \text{mass of } R_{j-1}); \quad j > 2$$

The equations of motion are obtained from Lagrange's equations for the six degree-of-freedom system where θ_j = inclination of the jth bar with the coordinate axes (Fig. 2).

The system of equations may be written as

$$A_{ij}\ddot{\theta}_j = B_i; \quad i, j = 1, 2, \ldots 6$$

where the A_{ij} coefficients and B_i terms are functions of $\dot{\theta}_n$,

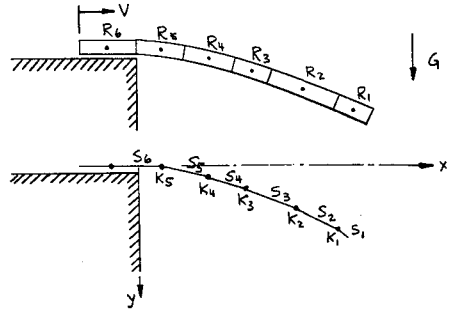

Fig. 2 Equivalent six-bar system.

Received May 11, 1970.

* Associate Director, Research and Development. Member AIAA.